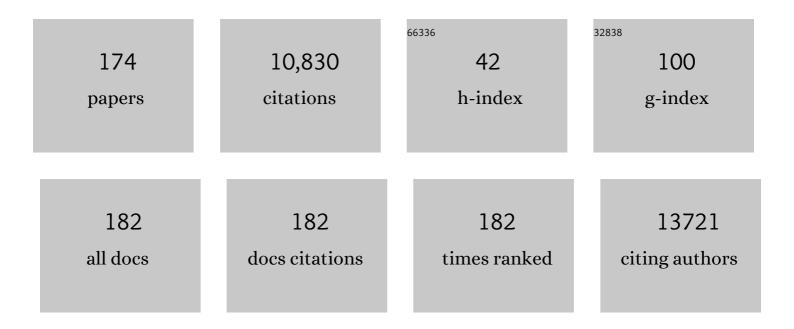
## Jin-Suck Suh

List of Publications by Year in descending order

Source: https://exaly.com/author-pdf/11157839/publications.pdf Version: 2024-02-01



IIN-SUCK SUH

#	Article	IF	CITATIONS
1	The Utility of Modified Dixon Turbo Spin Echo Shoulder Magnetic Resonance Arthrography in Assessing Rotator Cuff Disorder and Evaluating the Rotator Cuff Muscles. Academic Radiology, 2021, 28, 233-242.	2.5	1
2	Characterization of Proton-Irradiated Polyaniline Nanoparticles Using Terahertz Thermal Spectroscopy. Crystals, 2021, 11, 765.	2.2	2
3	Labeling-free detection of ECD-HER2 protein using aptamer-based nano-plasmonic sensor. Nanotechnology, 2020, 31, 175501.	2.6	7
4	Comprehensive Immuno-Molecular Profiles for Liposarcoma: Roles of Programmed Death Ligand 1, Microsatellite Instability, and PIK3CA. Oncology, 2020, 98, 817-826.	1.9	4
5	Accelerated metallic artifact reduction imaging using spectral bin modulation of multiacquisition variable-resonance image combination selective imaging. Magnetic Resonance Imaging, 2020, 72, 19-24.	1.8	4
6	Fast isotropic volumetric magnetic resonance imaging of the ankle: Acceleration of the three-dimensional fast spin echo sequence using compressed sensing combined with parallel imaging. European Journal of Radiology, 2019, 112, 52-58.	2.6	14
7	Bandgap-controlled hollow polyaniline nanostructures synthesized by Mn-dependent nano-confined polymerization. Nanoscale, 2019, 11, 2434-2438.	5.6	7
8	Detection of Keratinizing Squamous Cell Carcinoma of The Tongue Using Terahertz Reflection Imaging. , 2019, , .		0
9	Investigation of Keratinizing Squamous Cell Carcinoma of the Tongue Using Terahertz Reflection Imaging. Journal of Infrared, Millimeter, and Terahertz Waves, 2019, 40, 247-256.	2.2	15
10	Differences in the Efficacies of Pazopanib and Gemcitabine/Docetaxel as Second-Line Treatments for Metastatic Soft Tissue Sarcoma. Oncology, 2019, 96, 59-69.	1.9	14
11	Double-inversion recovery with synthetic magnetic resonance: a pilot study for assessing synovitis of the knee joint compared to contrast-enhanced magnetic resonance imaging. European Radiology, 2019, 29, 2573-2580.	4.5	19
12	Detection of vertebral metastases: a comparison between the modified Dixon turbo spin echo <i>T</i> <sub>2</sub> weighted MRI and conventional <i>T</i> <sub>1</sub> weighted MRI: a preliminary study in a tertiary centre. British Journal of Radiology, 2018, 91, 20170782.	2.2	22
13	Accelerating knee MR imaging: Compressed sensing in isotropic three-dimensional fast spin-echo sequence. Magnetic Resonance Imaging, 2018, 46, 90-97.	1.8	31
14	Comparison of T2â^— mapping between regular echo time and ultrashort echo time with 3D cones at 3 tesla for knee meniscus. Medicine (United States), 2018, 97, e13443.	1.0	3
15	Aptamer-modified Magnetic Nanosensitizer for in vivo MR imaging of HER2-expressing Cancer. Nanoscale Research Letters, 2018, 13, 288.	5.7	10
16	Charactering water Contents in Organ tissues Using THz Pulses. , 2018, , .		0
17	Microsphereâ€Based Nanoindentation for the Monitoring of Cellular Cortical Stiffness Regulated by MT1â€MMP. Small, 2018, 14, e1803000.	10.0	6
18	Measuring water contents in animal organ tissues using terahertz spectroscopic imaging. Biomedical Optics Express, 2018, 9, 1582.	2.9	30

#	Article	IF	CITATIONS
19	Study of molecular structure change of d- and l-glucose by proton irradiation using terahertz spectroscopy. Infrared Physics and Technology, 2018, 93, 154-157.	2.9	11
20	Articular cartilage grading of the knee: diagnostic performance of fat-suppressed 3D volume isotropic turbo spin-echo acquisition (VISTA) compared with 3D T1 high-resolution isovolumetric examination (THRIVE). Acta Radiologica, 2017, 58, 190-196.	1.1	12
21	Value of the Strain Ratio on Ultrasonic Elastography for Differentiation of Benign and Malignant Soft Tissue Tumors. Journal of Ultrasound in Medicine, 2017, 36, 121-127.	1.7	28
22	Reassessment of alkaline phosphatase as serum tumor marker with high specificity in osteosarcoma. Cancer Medicine, 2017, 6, 1311-1322.	2.8	48
23	Rapid acquisition of magnetic resonance imaging of the shoulder using three-dimensional fast spin echo sequence with compressed sensing. Magnetic Resonance Imaging, 2017, 42, 152-157.	1.8	30
24	Assessment of the patellofemoral cartilage: Correlation of knee pain score with magnetic resonance cartilage grading and magnetization transfer ratio asymmetry of glycosaminoglycan chemical exchange saturation transfer. Magnetic Resonance Imaging, 2017, 35, 61-68.	1.8	8
25	Three-Dimensional Fast Spin-Echo Imaging without Fat Suppression of the Knee: Diagnostic Accuracy Comparison to Fat-Suppressed Imaging on 1.5T MRI. Yonsei Medical Journal, 2017, 58, 1186.	2.2	6
26	The Effectiveness of Ferritin as a Contrast Agent for Cell Tracking MRI in Mouse Cancer Models. Yonsei Medical Journal, 2017, 58, 51.	2.2	6
27	Fat-suppressed MR Imaging of the Spine for Metal Artifact Reduction at 3T: Comparison of STIR and Slice Encoding for Metal Artifact Correction Fat-suppressed T <sub>2</sub> -weighted Images. Magnetic Resonance in Medical Sciences, 2016, 15, 371-378.	2.0	14
28	Prognostic Model to Predict Survival Outcome for Curatively Resected Liposarcoma: A Multi-Institutional Experience. Journal of Cancer, 2016, 7, 1174-1180.	2.5	25
29	Biomarker-specific conjugated nanopolyplexes for the active coloring of stem-like cancer cells. Nanotechnology, 2016, 27, 225101.	2.6	5
30	Photothermal ablation of cancer cells using self-doped polyaniline nanoparticles. Nanotechnology, 2016, 27, 185104.	2.6	26
31	Nanovesicle-mediated systemic delivery of microRNA-34a for CD44 overexpressing gastric cancer stem cell therapy. Biomaterials, 2016, 105, 12-24.	11.4	63
32	Terahertz reflectometry imaging for low and high grade gliomas. Scientific Reports, 2016, 6, 36040.	3.3	90
33	Fat fraction estimation of morphologically normal lumbar vertebrae using the two-point mDixon turbo spin-echo MRI with flexible echo times and multipeak spectral model of fat: Comparison between cancer and non-cancer patients. Magnetic Resonance Imaging, 2016, 34, 1114-1120.	1.8	16
34	Cancer theranosis using mono-disperse, mesoporous gold nanoparticles obtained via a robust, high-yield synthetic methodology. RSC Advances, 2016, 6, 13554-13561.	3.6	14
35	Femto-molar detection of cancer marker-protein based on immuno-nanoplasmonics at single-nanoparticle scale. Nanotechnology, 2016, 27, 185103.	2.6	8
36	Ultrashort echo (UTE) versus pointwise encoding time reduction with radial acquisition (PETRA) sequences at 3 Tesla for knee meniscus: A comparative study. Magnetic Resonance Imaging, 2016, 34, 75-80.	1.8	11

#	Article	IF	CITATIONS
37	Clinical value of fat-suppressed 3D volume isotropic spin-echo (VISTA) sequence compared to 2D sequence in evaluating internal structures of the knee. Acta Radiologica, 2016, 57, 66-73.	1.1	15
38	In vivo sensing of proteolytic activity with an NSET-based NIR fluorogenic nanosensor. Biosensors and Bioelectronics, 2016, 77, 471-477.	10.1	19
39	Absorption spectrum of gafchromic® EBT2 film with angular rotation. Journal of the Korean Physical Society, 2015, 67, 52-56.	0.7	1
40	Synthesis of Stable Magnetic Polyaniline Nanohybrids with Pyrene as a Cross-Linker for Simultaneous Diagnosis by Magnetic Resonance Imaging and Photothermal Therapy. European Journal of Inorganic Chemistry, 2015, 2015, 3740-3747.	2.0	12
41	Comparison of Multi-Echo Dixon Methods with Volume Interpolated Breath-Hold Gradient Echo Magnetic Resonance Imaging in Fat-Signal Fraction Quantification of Paravertebral Muscle. Korean Journal of Radiology, 2015, 16, 1086.	3.4	36
42	Compensatory UTE/T2W Imaging of Inflammatory Vascular Wall in Hyperlipidemic Rabbits. PLoS ONE, 2015, 10, e0124572.	2.5	2
43	T 2- and T*2-weighted MRI of rat glioma using polysorbate-coated magnetic nanocrystals as a blood-pool contrast agent. RSC Advances, 2015, 5, 19708-19714.	3.6	1
44	Spectral parametric segmentation of contrast-enhanced dual-energy CT to detect bone metastasis: feasibility sensitivity study using whole-body bone scintigraphy. Acta Radiologica, 2015, 56, 458-464.	1.1	13
45	Selfâ€Doped Conjugated Polymeric Nanoassembly by Simplified Process for Optical Cancer Theragnosis. Advanced Functional Materials, 2015, 25, 2260-2269.	14.9	20
46	Short T2 tissue imaging with the Pointwise Encoding Time reduction with Radial Acquisition (PETRA) sequence: The additional value of fat saturation and subtraction in the meniscus. Magnetic Resonance Imaging, 2015, 33, 385-389.	1.8	3
47	A systematic study of core size and coating thickness on manganese-doped nanocrystals for high T2 relaxivity as magnetic resonance contrast agent. Nano Convergence, 2015, 2, .	12.1	5
48	Galactosylated magnetic nanovectors for regulation of lipid metabolism based on biomarker-specific RNAi and MR imaging. Nanotechnology, 2015, 26, 335101.	2.6	1
49	Detection and Correction of Laterality Errors in Radiology Reports. Journal of Digital Imaging, 2015, 28, 412-416.	2.9	8
50	A new relative tumor sizing method in epi-metaphyseal osteosarcoma. BMC Cancer, 2015, 15, 284.	2.6	6
51	Colourimetric redox-polyaniline nanoindicator for in situ vesicular trafficking of intracellular transport. Nano Research, 2015, 8, 1169-1179.	10.4	8
52	Feasibility of terahertz reflectometry for discrimination of human early gastric cancers. Biomedical Optics Express, 2015, 6, 1398.	2.9	69
53	A magnetic polyaniline nanohybrid for MR imaging and redox sensing of cancer cells. Nanoscale, 2015, 7, 1661-1666.	5.6	14
54	MR Quantification of the Fatty Fraction from T2*-corrected Dixon Fat/Water Separation Volume-interpolated Breathhold Examination (VIBE) in the Assessment of Muscle Atrophy in Rotator Cuff Tears. Academic Radiology, 2015, 22, 909-917.	2.5	20

#	Article	IF	CITATIONS
55	Simple and Efficient Method for Region of Interest Value Extraction from Picture Archiving and Communication System Viewer with Optical Character Recognition Software and Macro Program. Academic Radiology, 2015, 22, 113-116.	2.5	5
56	One-pot synthesis of magnetic nanoclusters enabling atherosclerosis-targeted magnetic resonance imaging. International Journal of Nanomedicine, 2014, 9, 2489.	6.7	4
57	Dual-Energy Computed Tomography Arthrography of the Shoulder Joint Using Virtual Monochromatic Spectral Imaging: Optimal Dose of Contrast Agent and Monochromatic Energy Level. Korean Journal of Radiology, 2014, 15, 746.	3.4	7
58	Development of <sup>1</sup> H- <sup>31</sup> P Animal RF Coil for pH Measurement Using a Clinical MR Scanner. Journal of the Korean Society of Magnetic Resonance in Medicine, 2014, 18, 52.	0.1	2
59	Weighted subtraction in 3D ultrashort echo time (UTE) imaging for visualization of short T2 tissues of the knee. Acta Radiologica, 2014, 55, 454-461.	1.1	21
60	MR thermometry analysis program for laser- or high-intensity focused ultrasound (HIFU)-induced heating at a clinical MR scanner. Journal of the Korean Physical Society, 2014, 65, 2126-2131.	0.7	0
61	Study of freshly excised brain tissues using terahertz imaging. Biomedical Optics Express, 2014, 5, 2837.	2.9	145
62	Terahertz spectroscopic imaging and properties of gastrointestinal tract in a rat model. Biomedical Optics Express, 2014, 5, 4162.	2.9	32
63	Aptamer-conjugated magnetic nanoparticles enable efficient targeted detection of integrin αvβ3 via magnetic resonance imaging. Journal of Biomedical Materials Research - Part A, 2014, 102, 49-59.	4.0	31
64	Maleimidyl magnetic nanoplatform for facile molecular MRI. Nanotechnology, 2014, 25, 275102.	2.6	8
65	Magnetic Nanoclusters Engineered by Polymerâ€Controlled Selfâ€Assembly for the Accurate Diagnosis of Atherosclerotic Plaques via Magnetic Resonance Imaging. Macromolecular Bioscience, 2014, 14, 943-952.	4.1	16
66	Imidazolized magnetic nanovectors with endosome disrupting moieties for the intracellular delivery and imaging of siRNA. Journal of Materials Chemistry B, 2014, 2, 8566-8575.	5.8	9
67	Magnetic resonance visualization of surgical classification of rotator cuff tear: comparison with three-dimensional shoulder magnetic resonance arthrography at 3.0 T. Clinical Imaging, 2014, 38, 858-863.	1.5	9
68	Gadoliniumâ€Enriched Polyaniline Particles (GPAPs) for Simultaneous Diagnostic Imaging and Localized Photothermal Therapy of Epithelial Cancer. Advanced Healthcare Materials, 2014, 3, 1408-1414.	7.6	34
69	Use of strain ratio in evaluating superficial soft tissue tumors on ultrasonic elastography. Journal of Medical Ultrasonics (2001), 2014, 41, 319-323.	1.3	11
70	Feasibility of fat-saturated T2-weighted magnetic resonance imaging with slice encoding for metal artifact correction (SEMAC) at 3T. Magnetic Resonance Imaging, 2014, 32, 1001-1005.	1.8	16
71	Molecular recognition of proteolytic activity in metastatic cancer cells using fluorogenic gold nanoprobes. Biosensors and Bioelectronics, 2014, 57, 171-178.	10.1	15
72	Gadolinium-based nanoparticles for highly efficient T1-weighted magnetic resonance imaging. Nanotechnology, 2014, 25, 245103.	2.6	12

**Јім-**Suck Suh

#	Article	IF	CITATIONS
73	Efficient CD44-targeted magnetic resonance imaging (MRI) of breast cancer cells using hyaluronic acid (HA)-modified MnFe2O4 nanocrystals. Nanoscale Research Letters, 2013, 8, 149.	5.7	33
74	Double-ligand modulation for engineering magnetic nanoclusters. Nanoscale Research Letters, 2013, 8, 104.	5.7	11
75	Continuous Coaxial Electrohydrodynamic Atomization System for Waterâ€Stable Wrapping of Magnetic Nanoparticles. Small, 2013, 9, 2325-2330.	10.0	7
76	Ultrafast Spin-Resolved Spectroscopy Reveals Dominant Exciton Dynamics in Conducting Polymer Polyaniline. Journal of Physical Chemistry C, 2013, 117, 20371-20375.	3.1	8
77	Aptamer-conjugated gold nanorod for photothermal ablation of epidermal growth factor receptor-overexpressed epithelial cancer. Journal of Biomedical Optics, 2013, 19, 051203.	2.6	22
78	Aptamer-modified magnetic nanoprobe for molecular MR imaging of VEGFR2 on angiogenic vasculature. Nanoscale Research Letters, 2013, 8, 399.	5.7	39
79	A Biodegradable Polymersome Containing Bclâ€xL siRNA and Doxorubicin as a Dual Delivery Vehicle for a Synergistic Anticancer Effect. Macromolecular Bioscience, 2013, 13, 745-754.	4.1	46
80	Usefulness of slice encoding for metal artifact correction (SEMAC) for reducing metallic artifacts in 3-T MRI. Magnetic Resonance Imaging, 2013, 31, 703-706.	1.8	48
81	Ï€-Hyaluronan nanocarriers for CD44-targeted and pH-boosted aromatic drug delivery. Journal of Materials Chemistry B, 2013, 1, 5686.	5.8	19
82	CD44-specific supramolecular hydrogels for fluorescence molecular imaging of stem-like gastric cancer cells. Integrative Biology (United Kingdom), 2013, 5, 669.	1.3	21
83	Hyaluronic acid receptor-targetable imidazolized nanovectors for induction of gastric cancer cell death by RNA interference. Biomaterials, 2013, 34, 4327-4338.	11.4	36
84	Fat-suppressed volume isotropic turbo spin echo acquisition (VISTA) MR imaging in evaluating radial and root tears of the meniscus: Focusing on reader-defined axial reconstruction. European Journal of Radiology, 2013, 82, 2296-2302.	2.6	17
85	A Highly Crystalline Manganeseâ€Doped Iron Oxide Nanocontainer with Predesigned Void Volume and Shape for Theranostic Applications. Advanced Materials, 2013, 25, 3202-3208.	21.0	31
86	Intrinsic ligament and triangular fibrocartilage complex (TFCC) tears of the wrist: comparison of isovolumetric 3D-THRIVE sequence MR arthrography and conventional MR image at 3 T. Magnetic Resonance Imaging, 2013, 31, 221-226.	1.8	84
87	Chitosan-based intelligent theragnosis nanocomposites enable pH-sensitive drug release with MR-guided imaging for cancer therapy. Nanoscale Research Letters, 2013, 8, 467.	5.7	64
88	Galactosylated manganese ferrite nanoparticles for targeted MR imaging of asialoglycoprotein receptor. Nanotechnology, 2013, 24, 475103.	2.6	16
89	Measurement depth enhancement in terahertz imaging of biological tissues. Optics Express, 2013, 21, 21299.	3.4	82
90	Characterization of blood using terahertz waves. Journal of Biomedical Optics, 2013, 18, 107008.	2.6	38

#	Article	IF	CITATIONS
91	Localized surface plasmon resonance based nanobiosensor for biomarker detection of invasive cancer cells. Journal of Biomedical Optics, 2013, 19, 051202.	2.6	27
92	Aptamer-conjugated gold nanorod for photothermal ablation of EGFR-overexpressed epithelial cancer. , 2013, , .		0
93	Gold Nanorod-Mediated Photothermal Modulation for Localized Ablation of Cancer Cells. Journal of Nanomaterials, 2012, 2012, 1-7.	2.7	15
94	Effect of Ligand Structure on MnO Nanoparticles for Enhanced <i>T</i> <sub>1</sub> Magnetic Resonance Imaging of Inflammatory Macrophages. European Journal of Inorganic Chemistry, 2012, 2012, 5960-5965.	2.0	15
95	Quantitative Computed Tomography (QCT) as a Radiology Reporting Tool by Using Optical Character Recognition (OCR) and Macro Program. Journal of Digital Imaging, 2012, 25, 815-818.	2.9	4
96	Self-fabricated dextran-coated gold nanoparticles using pyrenyl dextran as a reducible stabilizer and their application as CT imaging agents for atherosclerosis. Journal of Materials Chemistry, 2012, 22, 17518.	6.7	25
97	Photo-thermal therapeutics control technique using terahertz waves. , 2012, , .		0
98	Br-Assisted Ostwald Ripening of Au Nanoparticles under H <sub>2</sub> O <sub>2</sub> Redox. Crystal Growth and Design, 2012, 12, 37-39.	3.0	38
99	Role of surface charge in cytotoxicity of charged manganese ferrite nanoparticles towards macrophages. Nanotechnology, 2012, 23, 505702.	2.6	29
100	Consecutive Targetable Smart Nanoprobe for Molecular Recognition of Cytoplasmic microRNA in Metastatic Breast Cancer. ACS Nano, 2012, 6, 8525-8535.	14.6	83
101	Medical application of THz imaging technique. , 2012, , .		3
102	Infrapatellar plica of the knee: Revisited with MR arthrographies undertaken in the knee flexion position mimicking operative arthroscopic posture. European Journal of Radiology, 2012, 81, 2783-2787.	2.6	16
103	Variations in dose distribution and optical properties of Gafchromic <sup>TM</sup> EBT2 film according to scanning mode. Medical Physics, 2012, 39, 2524-2535.	3.0	16
104	Highly selective CD44-specific gold nanorods for photothermal ablation of tumorigenic subpopulations generated in MCF7 mammospheres. Nanotechnology, 2012, 23, 465101.	2.6	20
105	Quantitative Assessment of Tumor Responses after Radiation Therapy in a DLD-1 Colon Cancer Mouse Model Using Serial Dynamic Contrast-Enhanced Magnetic Resonance Imaging. Yonsei Medical Journal, 2012, 53, 1147.	2.2	7
106	Targetable Gold Nanorods for Epithelial Cancer Therapy Guided by Nearâ€IR Absorption Imaging. Small, 2012, 8, 746-753.	10.0	98
107	Metal artefact reduction in gemstone spectral imaging dual-energy CT with and without metal artefact reduction software. European Radiology, 2012, 22, 1331-1340.	4.5	236
108	Anchored Proteinaseâ€Targetable Optomagnetic Nanoprobes for Molecular Imaging of Invasive Cancer Cells. Angewandte Chemie - International Edition, 2012, 51, 945-948.	13.8	42

#	Article	IF	CITATIONS
109	Cancer Diagnosis by Terahertz Molecular Imaging Technique. Journal of Infrared, Millimeter, and Terahertz Waves, 2012, 33, 74-81.	2.2	37
110	Molecular imaging with terahertz waves. Optics Express, 2011, 19, 4009.	3.4	87
111	Correlations of 3T DCE-MRI Quantitative Parameters with Microvessel Density in a Human-Colorectal-Cancer Xenograft Mouse Model. Korean Journal of Radiology, 2011, 12, 722.	3.4	20
112	Sensitive Angiogenesis Imaging of Orthotopic Bladder Tumors in Mice Using a Selective Magnetic Resonance Imaging Contrast Agent Containing VEGF121/rGel. Investigative Radiology, 2011, 46, 441-449.	6.2	35
113	Hyaluronan-modified magnetic nanoclusters for detection of CD44-overexpressing breast cancer by MR imaging. Biomaterials, 2011, 32, 7941-7950.	11.4	104
114	Dextran-coated magnetic nanoclusters as highly sensitive contrast agents for magnetic resonance imaging of inflammatory macrophages. Journal of Materials Chemistry, 2011, 21, 12473.	6.7	32
115	Characterization of blood cells by using terahertz waves. , 2011, , .		0
116	Specific Nearâ€IR Absorption Imaging of Glioblastomas Using Integrinâ€Targeting Gold Nanorods. Advanced Functional Materials, 2011, 21, 1082-1088.	14.9	71
117	pHâ€Triggered Drugâ€Releasing Magnetic Nanoparticles for Cancer Therapy Guided by Molecular Imaging by MRI. Advanced Materials, 2011, 23, 2436-2442.	21.0	194
118	Convertible Organic Nanoparticles for Nearâ€Infrared Photothermal Ablation of Cancer Cells. Angewandte Chemie - International Edition, 2011, 50, 441-444.	13.8	440
119	Urchinâ€Shaped Manganese Oxide Nanoparticles as pHâ€Responsive Activatable <i>T<sub>1</sub></i> Contrast Agents for Magnetic Resonance Imaging. Angewandte Chemie - International Edition, 2011, 50, 10589-10593.	13.8	141
120	Ambidextrous magnetic nanovectors for synchronous gene transfection and labeling of human MSCs. Biomaterials, 2011, 32, 6174-6182.	11.4	18
121	Gold Nanostructures as Photothermal Therapy Agent for Cancer. Anti-Cancer Agents in Medicinal Chemistry, 2011, 11, 953-964.	1.7	51
122	Terahertz pulse imaging of fresh brain tumor. , 2011, , .		7
123	Imaging of Nanoparticle Delivery Using Terahertz Waves. Fundamental Biomedical Technologies, 2011, , 701-711.	0.2	1
124	Prostate cancer cell death produced by the co-delivery of Bcl-xL shRNA and doxorubicin using an aptamer-conjugated polyplex. Biomaterials, 2010, 31, 4592-4599.	11.4	153
125	Magnetoplex based on MnFe2O4 nanocrystals for magnetic labeling and MR imaging of human mesenchymal stem cells. Journal of Nanoparticle Research, 2010, 12, 1275-1283.	1.9	9
126	Synthesis of aminated polysorbate 80 for polyplexâ€mediated gene transfection. Biotechnology Progress, 2010, 26, 1528-1533.	2.6	5

#	Article	IF	CITATIONS
127	Self-assembled fluorescent magnetic nanoprobes for multimode-biomedical imaging. Biomaterials, 2010, 31, 9310-9319.	11.4	52
128	Thiolated Dextran-Coated Gold Nanorods for Photothermal Ablation of Inflammatory Macrophages. Langmuir, 2010, 26, 17520-17527.	3.5	67
129	Nanomechanical In Situ Monitoring of Proteolysis of Peptide by Cathepsin B. PLoS ONE, 2009, 4, e6248.	2.5	26
130	A new terahertz technique for cancer diagnosis: T probe. , 2009, , .		0
131	The Usefulness of Virtual MR Arthroscopy as an Adjunct to Conventional MR Arthrography in Detecting Anterior Labral Lesions of the Shoulder. American Journal of Roentgenology, 2009, 192, W149-W155.	2.2	12
132	Gold-layered calcium phosphate plasmonic resonants for localized photothermal treatment of human epithelial cancer. Journal of Materials Chemistry, 2009, 19, 2902.	6.7	14
133	Smart Drugâ€Loaded Polymer Gold Nanoshells for Systemic and Localized Therapy of Human Epithelial Cancer. Advanced Materials, 2009, 21, 4339-4342.	21.0	151
134	Synthesis and characterization of fluorescent magneto polymeric nanoparticles (FMPNs) for bimodal imaging probes. Journal of Colloid and Interface Science, 2009, 340, 176-181.	9.4	10
135	Nanoparticle-enabled terahertz imaging for cancer diagnosis. Optics Express, 2009, 17, 3469.	3.4	161
136	Synthesis of gold nanorod-embedded polymeric nanoparticles by a nanoprecipitation method for use as photothermal agents. Nanotechnology, 2009, 20, 365602.	2.6	44
137	Self-labeled magneto nanoprobes using tri-aminated polysorbate 80 for detection of human mesenchymal stem cells. Journal of Materials Chemistry, 2009, 19, 8958.	6.7	21
138	Cancer-Targeted MR Molecular Imaging. Journal of the Korean Medical Association, 2009, 52, 121.	0.3	4
139	Enhancement of cellular binding efficiency and cytotoxicity using polyethylene glycol base triblock copolymeric nanoparticles for targeted drug delivery. Journal of Biomedical Materials Research - Part A, 2008, 84A, 273-280.	4.0	15
140	Enhancement of magnetic resonance contrast effect using ionic magnetic clusters. Journal of Colloid and Interface Science, 2008, 319, 429-434.	9.4	21
141	Fluorescent magnetic nanohybrids as multimodal imaging agents for human epithelial cancer detection. Biomaterials, 2008, 29, 2548-2555.	11.4	91
142	Synthesis of water soluble PEGylated magnetic complexes using mPEG-fatty acid for biomedical applications. Colloids and Surfaces B: Biointerfaces, 2008, 64, 111-117.	5.0	21
143	Hollow Silica Nanocontainers as Drug Delivery Vehicles. Langmuir, 2008, 24, 3417-3421.	3.5	230
144	Nanohybrids via a polycation-based nanoemulsion method for dual-mode detection of human mesenchymal stem cells. Journal of Materials Chemistry, 2008, 18, 4402.	6.7	12

#	Article	IF	CITATIONS
145	In Situ Detection of Live Cancer Cells by Using Bioprobes Based on Au Nanoparticles. Langmuir, 2008, 24, 12112-12115.	3.5	38
146	Smart nanoprobes for ultrasensitive detection of breast cancer via magnetic resonance imaging. Nanotechnology, 2008, 19, 485101.	2.6	22
147	Magnetic sensitivity enhanced novel fluorescent magnetic silica nanoparticles for biomedical applications. Nanotechnology, 2008, 19, 075610.	2.6	21
148	Nanoparticle contrast agents for Terahertz medical imaging. , 2008, , .		4
149	Ankle MRI for Anterolateral Soft Tissue Impingement: Increased Accuracy with the Use of Contrast-Enhanced Fat-Suppressed 3D-FSPGR MRI. Korean Journal of Radiology, 2008, 9, 409.	3.4	13
150	Chronic Tibiofibular Syndesmosis Injury of Ankle: Evaluation with Contrast-enhanced Fat-suppressed 3D Fast Spoiled Gradient-recalled Acquisition in the Steady State MR Imaging. Radiology, 2007, 242, 225-235.	7.3	44
151	Novel multifunctional PHDCA/PEI nano-drug carriers for simultaneous magnetically targeted cancer therapy and diagnosis via magnetic resonance imaging. Nanotechnology, 2007, 18, 475105.	2.6	32
152	Chronic Tibiofibular Syndesmosis Injury: The Diagnostic Efficiency of Magnetic Resonance Imaging and Comparative Analysis of Operative Treatment. Foot and Ankle International, 2007, 28, 336-342.	2.3	147
153	Overcoming Artifacts from Metallic Orthopedic Implants at High-Field-Strength MR Imaging and Multi-detector CT. Radiographics, 2007, 27, 791-803.	3.3	479
154	Antibody conjugated magnetic PLGA nanoparticles for diagnosis and treatment of breast cancer. Journal of Materials Chemistry, 2007, 17, 2695.	6.7	176
155	Synthesis of Ultrasensitive Magnetic Resonance Contrast Agents for Cancer Imaging Using PEG-Fatty Acid. Chemistry of Materials, 2007, 19, 3870-3876.	6.7	73
156	Multifunctional Magnetoâ€₽olymeric Nanohybrids for Targeted Detection and Synergistic Therapeutic Effects on Breast Cancer. Angewandte Chemie - International Edition, 2007, 46, 8836-8839.	13.8	311
157	Artificially engineered magnetic nanoparticles for ultra-sensitive molecular imaging. Nature Medicine, 2007, 13, 95-99.	30.7	1,756
158	A calorimetric biosensor and its application for detecting a cancer cell with optical imaging. , 2007, , 637-640.		9
159	In vivo MR Imaging of Tissue-engineered Human Mesenchymal Stem Cells Transplanted to Mouse: a Preliminary Study. Annals of Biomedical Engineering, 2006, 35, 101-108.	2.5	37
160	Anterior-inferior labral lesions of recurrent shoulder dislocation evaluated by MR arthrography in an adduction internal rotation (ADIR) position. Journal of Magnetic Resonance Imaging, 2006, 23, 29-35.	3.4	48
161	Nanoscale Size Effect of Magnetic Nanocrystals and Their Utilization for Cancer Diagnosis via Magnetic Resonance Imaging. Journal of the American Chemical Society, 2005, 127, 5732-5733.	13.7	1,131
162	Tumor Volume Change after Chemotheraphy as a Predictive Factor of Disease Free Survival for Osteosarcoma. Yonsei Medical Journal, 2005, 46, 119.	2.2	8

#	Article	IF	CITATIONS
163	The Role of Popliteal Lymph Nodes in Differentiating Rheumatoid Arthritis from Osteoarthritis by Using CE 3D-FSPGR MR Imaging: Relationship of the Inflamed Synovial Volume. Korean Journal of Radiology, 2005, 6, 117.	3.4	16
164	Surface Modulation of Magnetic Nanocrystals in the Development of Highly Efficient Magnetic Resonance Probes for Intracellular Labeling. Journal of the American Chemical Society, 2005, 127, 9992-9993.	13.7	299
165	In Vivo Magnetic Resonance Detection of Cancer by Using Multifunctional Magnetic Nanocrystals. Journal of the American Chemical Society, 2005, 127, 12387-12391.	13.7	829
166	Soft Tissue Impingement Syndrome of the Ankle: Diagnostic Efficacy of MRI and Clinical Results after Arthroscopic Treatment. Foot and Ankle International, 2004, 25, 896-902.	2.3	47
167	Synovitis and soft tissue impingement of the ankle: Assessment with enhanced three-dimensional FSPGR MR imaging. Journal of Magnetic Resonance Imaging, 2004, 19, 108-116.	3.4	36
168	MR Evaluation of Radiation Synovectomy of the Knee by Means of Intra-articular Injection of Holmium-166-Chitosan Complex in Patients with Rheumatoid Arthritis: Results at 4-month Follow-up. Korean Journal of Radiology, 2003, 4, 170.	3.4	32
169	Magnetic resonance imaging of articular cartilage. European Radiology, 2001, 11, 2015-2025.	4.5	30
170	Tumor Volume Change as a Predictor of Chemotherapeutic Response in Osteosarcoma. Clinical Orthopaedics and Related Research, 2000, 376, 200-208.	1.5	63
171	Role of the inflamed synovial volume of the wrist in defining remission of rheumatoid arthritis with gadolinium-enhanced 3D-SPGR MR imaging. Journal of Magnetic Resonance Imaging, 1999, 10, 202-208.	3.4	27
172	Chondromalacia of the knee: Evaluation with a fat-suppression three-dimensional SPGR imaging after intravenous contrast injection. Journal of Magnetic Resonance Imaging, 1996, 6, 884-888.	3.4	27
173	The use of MRI in the diagnosis of benign and malignant bone and soft tissue tumours. Journal of Medical Imaging and Radiation Oncology, 1993, 37, 35-39.	0.6	9
174	Bursitis in association with solitary osteochondromas presenting as mass lesions. Skeletal Radiology, 1991, 20, 513-516.	2.0	59